



HAL
open science

Terahertz spectroscopy of the 15 NH_2 amidogen radical

L. Margulès, M. Martin-Drumel, O. Pirali, S. Bailleux, G. Wlodarczak, Pascal Roy, E. Roueff, M. Gerin

► **To cite this version:**

L. Margulès, M. Martin-Drumel, O. Pirali, S. Bailleux, G. Wlodarczak, et al.. Terahertz spectroscopy of the 15 NH_2 amidogen radical. *Astronomy and Astrophysics - A&A*, 2016, 591, pp.A110. 10.1051/0004-6361/201628201 . hal-02431838

HAL Id: hal-02431838

<https://hal.science/hal-02431838>

Submitted on 2 Nov 2022

HAL is a multi-disciplinary open access archive for the deposit and dissemination of scientific research documents, whether they are published or not. The documents may come from teaching and research institutions in France or abroad, or from public or private research centers.

L'archive ouverte pluridisciplinaire **HAL**, est destinée au dépôt et à la diffusion de documents scientifiques de niveau recherche, publiés ou non, émanant des établissements d'enseignement et de recherche français ou étrangers, des laboratoires publics ou privés.

Terahertz spectroscopy of the $^{15}\text{NH}_2$ amidogen radical[★]

L. Margulès¹, M. A. Martin-Drumel^{2,3,★★}, O. Pirali^{2,3}, S. Bailleux¹, G. Wlodarczak¹, P. Roy²,
E. Roueff⁴, and M. Gerin⁵

¹ Univ. Lille, CNRS, UMR 8523 – PhLAM – Physique des Lasers, Atomes et Molécules, 59000 Lille, France
e-mail: laurent.margules@univ-lille1.fr

² SOLEIL Synchrotron, AILES beamline, l’Orme des Merisiers, Saint-Aubin, 91192 Gif-sur-Yvette Cedex, France

³ Institut des Sciences Moléculaires d’Orsay (ISMO), CNRS, Univ. Paris-Sud, Université Paris-Saclay, 91405 Orsay, France

⁴ LERMA, Observatoire de Paris, PSL Research University, CNRS, Sorbonne Universités, UPMC Univ. Paris 06, 92190 Meudon, France

⁵ LERMA, UMR 8112 CNRS, 24 Rue Lhomond, 75231 Paris Cedex 05, France

Received 27 January 2016 / Accepted 31 March 2016

ABSTRACT

Context. The determination of isotopic ratios in interstellar molecules is a powerful probe of chemical routes leading to their formation. In particular, the $^{14}\text{N}/^{15}\text{N}$ abundance ratio of nitrogen-bearing species provides information on possible fractionation mechanisms. Up to now there is no accurate determination of this ratio in the interstellar medium (ISM) for the amidogen radical, NH_2 .

Aims. This work is aimed at determining rotational frequencies of $^{15}\text{NH}_2$ to enable its astronomical detection, which will help to understand the formation mechanisms of nitrogen hydrides in the ISM.

Methods. We performed complementary measurements using both synchrotron-based, broadband far-infrared and high-resolution, submillimeter-wave frequencies to investigate the pure rotational spectrum of the $^{15}\text{NH}_2$ species.

Results. The first spectroscopic study of the ^{15}N -isotopologue of the amidogen radical yielded an accurate set of molecular parameters.

Conclusions. Accurate frequencies are now available for $^{15}\text{NH}_2$ up to 7 THz (with $N'' \leq 13$) allowing dedicated astronomical searches to be undertaken.

Key words. submillimeter: ISM – line: identification – astronomical databases: miscellaneous – ISM: molecules

1. Introduction

The formation mechanism of most of the complex organic molecules being still unknown, the determination of isotopic ratios in the interstellar medium (ISM) is a great help to improve knowledge about their formation process. The $^{14}\text{N}/^{15}\text{N}$ ratio is less characterized than H/D or $^{12}\text{C}/^{13}\text{C}$ ratios. Using the $N = 1-0$ pattern for CN, HCN, and HNC at 3 mm, Adande & Ziurys (2012) retrieved the $^{14}\text{N}/^{15}\text{N}$ ratio and its gradient towards 11 molecular clouds spanning a wide range of distances from the Galactic center that are representative of star-forming regions. Isotopic ratios are also used to test the link between cometary and interstellar molecules as reviewed recently by Mumma & Charnley (2011). Hily-Blant et al. (2013b) used CN transitions to study the $^{14}\text{N}/^{15}\text{N}$ ratio isotopic ratio in two dark clouds, whereas Hily-Blant et al. (2013a) discussed ^{15}N enrichment in the dark clouds L1544 and L1498 and solar system objects and raised a possible chemical origin for the observational differences between nitriles and nitrogen hydrides (misleadingly called amines by these authors). We also mention the detection of HC^{15}N in the extragalactic Arp220 environment. Recently, Füri & Marty (2015) suggested that the variation of

nitrogen isotopic ratio offers a powerful tracer for investigating the origins of planetary atmospheres.

The present study offers an additional possibility to measure the $^{14}\text{N}/^{15}\text{N}$ abundance ratio in the NH_2 amidogen molecule. NH_2 has been detected in its ortho and para forms as a result of its absorption transitions in the submillimeter region towards high-mass star-forming regions W31C, W49N, W51, and G34.3 (Persson et al. 2012, 2016) with a relative abundance compared to molecular hydrogen of several 10^{-9} in the molecular envelopes. This nitrogen hydride witnesses the chain of formation reactions involving molecular hydrogen, starting with $\text{N}^+ + \text{H}_2$ and terminating in NH_4^+ from which NH_2 and NH_3 are produced through dissociative recombination. The $^{14}\text{N}/^{15}\text{N}$ ratio in NH_2 and NH_3 depends on the ortho/para ratio of molecular hydrogen, which triggers the initial step as discussed in Dislaire et al. (2012) and Roueff et al. (2015). It should be stressed that the $^{14}\text{N}/^{15}\text{N}$ isotopic ratio of NH_3 and NH_2D were determined in the B1 dark molecular cloud (Lis et al. 2010; Gerin et al. 2009; Daniel et al. 2013) and are satisfactorily explained through gas-phase chemistry (Roueff et al. 2015). However, present models fail to explain the large depletions of ^{15}N found in the two isotopologues of N_2H^+ (Bizzocchi et al. 2010, 2013; Fontani et al. 2015). It is finally worth mentioning the recent detection of $^{15}\text{NH}_2$ in two comets (Rousselot et al. 2014; Shinnaka et al. 2014) thanks to visible spectroscopy that allowed the authors to derive a $^{14}\text{N}/^{15}\text{N}$ ratio of 127 for NH_2 , which is similar to the ratio observed for HCN/CN molecules in these objects. This first detection in comets is indeed very encouraging for interstellar

[★] Full Table 2 (S1) and fitting files (S2-S4) are only available at the CDS via anonymous ftp to cdsarc.u-strasbg.fr (130.79.128.5) or via

<http://cdsarc.u-strasbg.fr/viz-bin/qcat?J/A+A/591/A110>

^{★★} Present address: Harvard-Smithsonian Center for Astrophysics, Cambridge, MA 02139, USA.

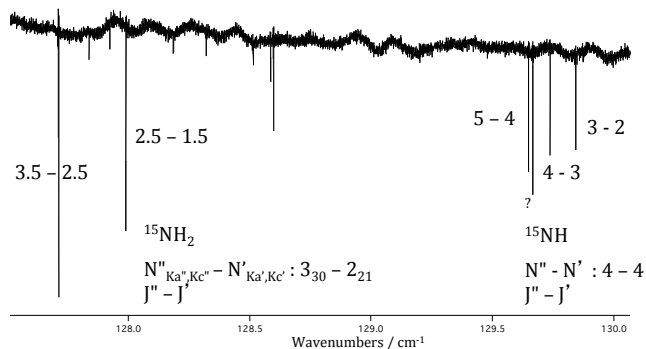


Fig. 1. Portion of the FT-FIR spectrum recorded using $^{15}\text{NH}_3$ as precursor: both $^{15}\text{NH}_2$ and ^{15}NH are simultaneously produced in the discharge.

studies as well. The present measurement of the first rotational lines of $^{15}\text{NH}_2$, around 640 GHz, is mandatory for its detection in the ISM using the very sensitive ALMA facility.

A strength of this project lies in the complementary measurements that were performed using synchrotron-based, far-infrared (FIR) and submillimeter spectroscopy to determine accurate frequencies over a wide spectral region (550–6000 GHz/18–200 cm^{-1}); these measurements are suitable for detection in the ISM.

2. Experiments

2.1. Production of the radical

The $^{15}\text{NH}_2$ radical was generated in a positive column discharge using $^{15}\text{NH}_3$ as a precursor (98%; Cambridge Isotope Laboratories, Inc.). Two such discharge cells were used for Fourier-transform FIR (FT-FIR) and submillimeter-wave spectroscopy. A description of the cells can be found in [Martin-Drumel et al. \(2011\)](#) and [Ozeki et al. \(2011\)](#), respectively. Briefly, for FT-FIR spectroscopy the 1-m-long, White-type cell available at SOLEIL allowed a 24 m absorption path length in the positive column of the discharge. For submillimeter-wave measurements (PhLAM laboratory), the single path discharge cell was 2 m long. He (1.26 mbar) and Ar (18 μbar) were used as buffer gas for a total pressure of 1 mbar and 25 μbar , respectively. The discharge current sustained between the water-cooled electrodes in the corresponding experimental set-ups was adjusted to 100 mA and 65 mA, respectively.

2.2. Synchrotron-based FT-FIR spectroscopy

The rotational spectrum of $^{15}\text{NH}_2$ has been investigated below 225 cm^{-1} (~ 7 THz) at the AILES beamline of SOLEIL synchrotron ([Brubach et al. 2010](#)) with a Bruker IFS125HR Fourier transform spectrometer making use of the high sensitivity and wide spectral range of the synchrotron radiation. The high-resolution (0.001 cm^{-1} or 30 MHz) FT-FIR spectrum of the radical was recorded using a 6 μm -thick Mylar beamsplitter and a 4.2 K liquid helium cooled Si-bolometer equipped with a 8 THz low-pass optical filter. The spectrum is the result of about seven hours of integration time (120 co-averaged interferograms). The spectrum was calibrated using residual H_2O lines against accurate frequencies from [Matsushima et al. \(1995\)](#) allowing a 0.0001 cm^{-1} measurement accuracy of $^{15}\text{NH}_2$ experimental frequencies. In addition, pure rotational transitions

of $^{15}\text{NH}_2$, absorption features of ^{15}NH – which was analysed in [Baillieux et al. \(2012\)](#) – and residual $^{15}\text{NH}_3$, $^{14}\text{NH}_3$, $^{14}\text{NH}_2$, ^{14}NH , H_2O , and OH are also visible (see [Martin-Drumel et al. 2014](#), Fig. 1).

2.3. Submillimeter-wave spectroscopy

In the 580–660 GHz frequency range, a backwards wave oscillator (BWO; Istok company) was used as a source of radiation. It was phase-locked to a harmonic of an Agilent E8257D synthesizer (2–20 GHz) ([Ozeki et al. 2011](#)). Additional measurements between 660 and 990 GHz were performed using a solid state source ([Motiyenko et al. 2010](#)). In this case, the frequency of the Agilent synthesizer fed a Spacek active sextupler providing an output power of +15 dBm in the W-band range (75–110 GHz). This power is high enough to use passive Schottky multipliers ($\times 6$ and $\times 9$ from Virginia Diodes, Inc.) in the next stage of the frequency multiplication chain. Both types of sources were frequency modulated at 10 kHz. A very sensitive InSb liquid, He-cooled bolometer (QMC Instruments Ltd) was used for detection.

With a total pressure of 25 μbar the linewidths were limited by Doppler broadening. As a result, isolated lines were measured with an accuracy better than 30 kHz, while blended lines and those observed with a poor signal-to-noise ratio were given an accuracy of 100 or 200 kHz.

3. Analysis of the rotational spectrum

3.1. Theory

The NH_2 radical in its ground electronic state (\widetilde{X}^2B_1) is a very asymmetric prolate rotor with an asymmetry parameter $\kappa = -0.374$. The 1.82 D dipole moment lies along the b -axis ([Brown et al. 1979](#)). There are many high-resolution spectroscopic studies concerning the amidogen radical in different wavelengths domains. A summary of the spectroscopic history can be found in the latest rotational spectroscopy study ([Martin-Drumel et al. 2014](#)). Although the deuterated species were studied ([Morino & Kawaguchi 1997](#); [Kobayashi et al. 1997](#)), there has been no investigation concerning the ^{15}N isotopologue until now.

Each rotational level with $N > 0$ is split into two sublevels because of the spin S of the unpaired electron. There is only one spin sublevel if $N = 0$ (corresponding to $J = \frac{1}{2}$). These fine structure levels are further split because of the nuclear spin of ^{15}N ($I_N = \frac{1}{2}$). Finally, the two equivalent hydrogen nuclei ($I_{\text{H}_1} = I_{\text{H}_2} = \frac{1}{2}$) give additional splitting of each of these sublevels for rotational levels with even $K_a + K_c$ (ortho levels), whereas no further splitting is observed with odd $K_a + K_c$ (para levels). These properties mean that the energy level diagram of $^{15}\text{NH}_2$ is similar to that of PH_2 . The representation of the resulting energy level diagram for the ortho levels can be found in Fig. 2 of [Margulès et al. \(2002\)](#). The rotational and spin angular momenta of $^{15}\text{NH}_2$ are coupled in the following way:

$$\mathbf{J} = \mathbf{N} + \mathbf{S} \quad (1)$$

$$\mathbf{F}_1 = \mathbf{J} + \mathbf{I}_N$$

$$\mathbf{F} = \mathbf{F}_1 + \mathbf{I}_H$$

with: $\mathbf{I}_H = \mathbf{I}_{\text{H}_1} + \mathbf{I}_{\text{H}_2}$.

Following the coupling scheme above, each level is characterized with the following set of quantum numbers: N, K_a, K_c, J, F_1, F . Pickett's programs SPFIT and SPCAT

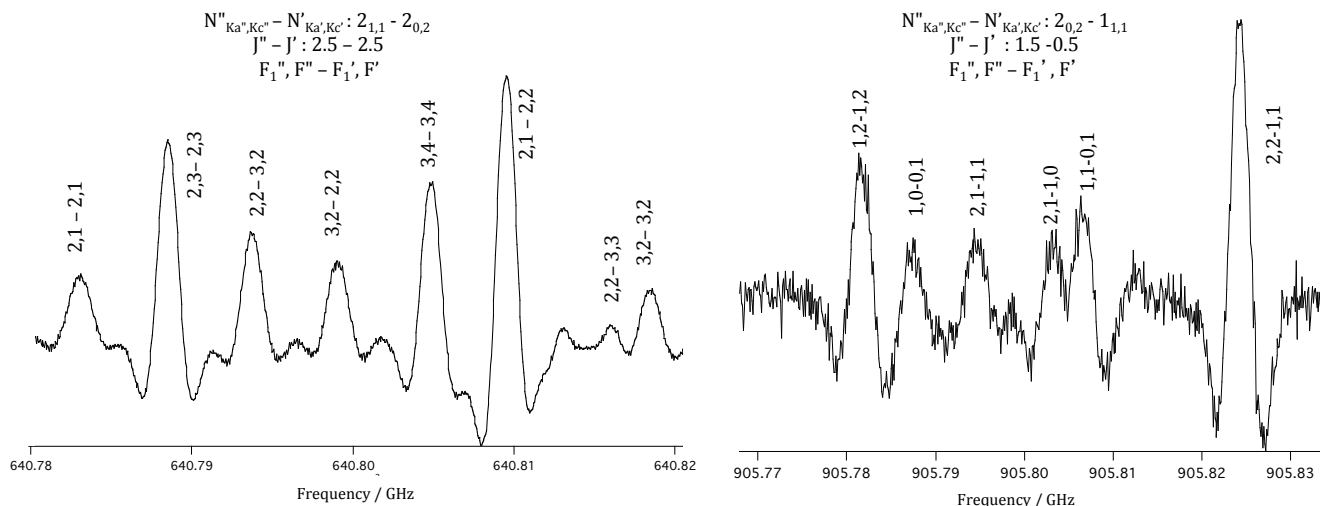


Fig. 2. Example of hyperfine splittings due to ^{15}N and H resolved in the submillimeter-wave spectrum. The lineshape appears as second derivative due to frequency modulation at $f = 10$ kHz and detection at $2f$.

were employed for fitting and predicting the spectra (Pickett 1991). The decomposition of the Hamiltonian is the same as that used in previous studies of NH_2 (Müller et al. 1999; Gendriesch et al. 2001; Martin-Drumel et al. 2014) and PH_2 (Margulès et al. 2002), i.e.

$$\mathcal{H} = \mathcal{H}_{\text{rot}} + \mathcal{H}_{\text{fs}} + \mathcal{H}_{\text{hfs}}. \quad (2)$$

The value \mathcal{H}_{rot} is the Watson A -reduced rotational Hamiltonian in the I' representation. In the present investigation, it contains centrifugal distortion constants up to the eighth order. The octic terms, which could not be determined, were kept fixed at the $^{14}\text{NH}_2$ value (Martin-Drumel et al. 2014). Quartic, sextic, and octic centrifugal distortion terms have also been included in the fine structure Hamiltonian \mathcal{H}_{fs} .

The hyperfine structure Hamiltonian \mathcal{H}_{hfs} can be separated into three parts:

$$\mathcal{H}_{\text{hfs}} = \mathcal{H}_{\text{esns}}(\text{N}) + \mathcal{H}_{\text{nsr}}(\text{N}) + \mathcal{H}_{\text{esns}}(\text{H}). \quad (3)$$

The first and third terms describe the electron spin-nuclear spin couplings between the electronic spin (es) and the nuclear spins (ns). The second term represents the nuclear spin-rotation (nsr) interactions caused by the nitrogen and hydrogen nuclei. As previously found in $^{14}\text{NH}_2$, other terms concerning the nuclear spin-rotation interactions and the electron spin-nuclear spin couplings were found to be insignificant.

3.2. Assignment

The initial prediction was made with a somewhat rough method. Rotational constants for both ^{14}N and ^{15}N amidogen radicals were first inferred from the r_0 structure deduced from the FT-FIR study (0.0075 cm^{-1} resolution) of NH_2 , NHD , and ND_2 by Morino & Kawaguchi (1997). These calculated constants are referred to as $B_{\text{par}}^{r_0}$ and $B_{\text{iso}}^{r_0}$, respectively, where B stands for the A , B , or C rotational constant of the parent (par) and isotologue (iso) species. The $^{15}\text{NH}_2$ rotational constants, noted as $B_{\text{iso}}^{\text{est}}$, were precisely estimated by correcting the three $B_{\text{iso}}^{r_0}$ with the $(B_{\text{par}}^{r_0} - B_{\text{par}}^{\text{exp}})$ differences, where $B_{\text{par}}^{\text{exp}}$ are the experimentally determined rotational constants of $^{14}\text{NH}_2$ from Müller et al. (1999): $B_{\text{iso}}^{\text{est}} = B_{\text{iso}}^{r_0} + (B_{\text{par}}^{r_0} - B_{\text{par}}^{\text{exp}})$. This method yields $^{15}\text{NH}_2$ estimated rotational constants with an accuracy better than 30 MHz (0.01%

on C). The centrifugal distortion and fine structure terms were fixed at their corresponding $^{14}\text{NH}_2$ values. The hyperfine parameters related to the ^{15}N nucleus were obtained by applying the gyromagnetic corrections to the related $^{14}\text{NH}_2$ parameters, as in our ^{15}NH previous study (Baillieux et al. 2012).

This prediction was accurate enough to readily assign and fit 142 lines in the FT-FIR spectrum ($N'' \leq 13$ and $K''_a \leq 5$). A zoom of the region around 129 cm^{-1} gives an example of the fine structures of $^{15}\text{NH}_2$ and ^{15}NH rotational transitions observed, 12 of which exhibit a resolved-nitrogen, hyperfine structure. A preliminary fit of these data enabled a prediction that was better than a few MHz in the submillimeter-wave region, resulting in a straightforward analysis of the corresponding transition frequencies. The hyperfine structure due to the hydrogen spins was resolved owing to the higher resolution achieved in this spectral region, as shown in Fig. 2. Seventy-seven additional lines, with $N'' \leq 5$ and $K''_a \leq 3$, were assigned and fitted.

Spectroscopic parameters of $^{15}\text{NH}_2$ were derived from a global fit of a total of 219 lines. A root mean square (rms) deviation of $1.0 \times 10^{-4} \text{ cm}^{-1}$ for the FT-FIR lines and 115 kHz for the submillimeter-wave lines was achieved (see Table 1). The list of measured rotational lines that are potential candidates for detection with the ALMA facility is provided in Table 2. Owing to its large size, the complete version of the global fit Table (S1) is supplied at the CDS. The fitting files .lin (S2), .par (S3), and the prediction .cat (S4) are also available at CDS.

4. Conclusion

The first high-resolution rotational spectroscopic study of $^{15}\text{NH}_2$ was performed using synchrotron-based broad range FIR measurements and submillimeter spectroscopy. A large number of lines were fitted within the experimental accuracy. Accurate frequencies of $^{15}\text{NH}_2$ can now be predicted up to at least 7 THz. The rotational transition $2_{1,1} - 2_{0,2}$ lies near 645 GHz and is therefore a good candidate for a possible detection with ALMA.

Acknowledgements. This work was supported by the Programme National ‘‘Physique et Chimie du Milieu Interstellaire’’ and the Centre National d’Études Spatiales (CNES). This work was also done under ANR-13-BS05-0008-02 IMOLABS. The authors are grateful to SOLEIL for providing beam time on the AILES beamline under the proposal 20110017.

Table 1. Spectroscopic parameters of the $^{15}\text{NH}_2$ and $^{14}\text{NH}_2$ radicals in their ground vibronic state.

Parameter in MHz	$^{15}\text{NH}_2$	$^{14}\text{NH}_2^a$
Rotational and centrifugal distortion constants		
A	704 388.406(45) ^b	710 302.019(10)
B	388 292.32(11)	388 289.458(15)
C	244 293.59(12)	245 013.520(11)
Δ_K	649.370(34)	659.7470(33)
Δ_{NK}	-124.365(18)	-125.1228(16)
Δ_N	31.6626(24)	31.68194(44)
δ_K	28.732(70)	29.6553(65)
δ_N	12.7139(15)	12.70818(17)
Φ_K	1.9178(28)	1.99230(42)
Φ_{KN}	-0.2739(27)	-0.28242(48)
Φ_{NK}	-0.04960(89)	-0.04888(15)
Φ_N	0.012841(66)	0.0128969(81)
ϕ_K	0.507(11)	0.52551(69)
ϕ_{NK}	-0.01624(33)	-0.016015(67)
$\phi_N \times 10^{-3}$	6.409(32)	6.4313(43)
$L_K \times 10^{-3}$	-8.63(24)	-10.665(22)
$L_{KKN} \times 10^{-3}$	3.70(37)	3.755(16)
$L_{NK} \times 10^{-3}$	-1.03(15)	-0.9976(57)
$L_{NNK} \times 10^{-3}$	0.0615(37)	0.057(14)
$L_N \times 10^{-6}$	-6.80(56)	-7.993(81)
$l_K \times 10^{-3}$	-3.63(34)	-4.145(15)
$l_{KN} \times 10^{-6}$	108.4 ^c	108.4(38)
$l_{NK} \times 10^{-6}$	8.03 ^c	8.03(35)
$l_N \times 10^{-6}$	-3.45(29)	-4.031(43)
Fine structure constants		
ϵ_{aa}	-9188.74(10)	-9267.840(26)
ϵ_{bb}	-1353.75(14)	-1354.194(14)
ϵ_{cc}	11.89(13)	12.220(15)
Δ_K^S	33.110(76)	34.0205(72)
$\Delta_{KN}^S + \Delta_{NK}^S$	-3.200(45)	-3.4938(67)
Δ_{NK}^S	15.7(22)	0.950(85)
Δ_N^S	0.3067(46)	0.31386(48)
δ_K^S	0.451(45)	0.5667(51)
δ_N^S	0.1474(24)	0.15716(24)
Φ_K^S	-0.1817(35)	-0.19276(70)
Φ_{NK}^S	0.0225(26)	0.02695(67)
ϕ_K^S	-0.01032 ^c	-0.01032(69)
$L_K^S \times 10^{-3}$	0.920 ^c	0.920(13)
$L_{KKN}^S \times 10^{-3}$	-0.144 ^c	-0.144(11)
Hyperfine structure constants		
$a_F(N)$	-39.275(69)	28.066(10)
$T_{aa}(N)$	60.34(15)	-43.175(16)
$T_{bb}(N)$	62.19(11)	-44.453(18)
$C_{aa}(N)$	-0.661(75)	0.4618(64)
$C_{bb}(N)$	-0.161(32)	0.0941(52)
$C_{cc}(N)$	-0.01501 ^d	0.0107(37)
$a_F(H)$	-67.187(34)	-67.184(11)
$T_{aa}(H)$	18.577(76)	18.333(20)
$T_{bb}(H)$	-13.248(62)	-13.161(22)
$T_{ab}(H)$	58.50 ^e	58.50 ^e
$C_{aa}(H)$	0.2183 ^c	0.2183(78)
$C_{bb}(H) \times 10^{-3}$	-6.8 ^d	-6.8(65)
$C_{cc}(H)$	-0.0248 ^d	-0.0248(50)
Number of FT-FIR lines (62–227 cm^{-1})		142
Standard deviation of the FT-FIR data (in cm^{-1})		1.0×10^{-4}
Number of submillimeter lines (150–660 GHz)		77
Standard deviation of the submillimeter data (in kHz)		115.5
$N''_{\max}, K''_{a\max}$		13, 5
Weighted deviation of fit		0.88

Notes. ^(a) $^{14}\text{NH}_2$ parameters are from [Martin-Drumel et al. \(2014\)](#). ^(b) Number in parenthesis is one standard deviation in unit of the last digit. ^(c) Fixed at the $^{14}\text{NH}_2$ value. ^(d) Fixed at the value from [Gendriesch et al. \(2001\)](#). ^(e) Fixed at the value from [Steimle et al. \(1980\)](#).

Table 2. Measured frequencies of the $2_{1,1}-2_{0,2}$ transition, and residuals from the global fit of the Infrared, and submillimeter-wave data for $^{15}\text{NH}_2$.

Upper level							Lower level							Frequency(Unc.)	O.-C.
N''	K''_a	K''_c	J''^a	F''_1^a	I''_H	F''^a	N'	K'_a	K'_c	J'^a	F'_1^a	I'_H	F'^a	(in MHz)	(in MHz)
2	1	1	3	3	1	4	2	0	2	2	2	1	3	639 001.675(0.100)	0.01381
2	1	1	3	2	1	3	2	0	2	2	2	1	2	639 045.833(0.100)	-0.01377
2	1	1	3	3	1	3	2	0	2	2	2	1	3	639 051.520(0.100)	-0.06082
2	1	1	3	2	1	3	2	0	2	2	1	1	2	639 076.520(0.100)	0.15477
2	1	1	3	3	1	3	2	0	2	2	2	1	2	639 083.185(0.100)	-0.05989
2	1	1	3	2	1	3	2	0	2	3	2	1	2	640 725.613(0.100)	0.01293
2	1	1	3	2	1	3	2	0	2	3	3	1	2	640 744.982(0.100)	0.05757
2	1	1	3	2	1	2	2	0	2	3	2	1	1	640 746.216(0.100)	-0.00670
2	1	1	3	3	1	4	2	0	2	3	3	1	3	640 754.822(0.100)	-0.09119
2	1	1	3	3	1	3	2	0	2	3	2	1	2	640 763.042(0.100)	0.04531
2	1	1	3	2	1	3	2	0	2	3	3	1	3	640 767.442(0.100)	0.00550
2	1	1	3	3	1	2	2	0	2	3	2	1	1	640 770.846(0.100)	0.02358
2	1	1	3	2	1	2	2	0	2	3	2	1	2	640 774.637(0.100)	0.20803
2	1	1	3	2	1	1	2	0	2	3	2	1	1	640 783.056(0.100)	-0.02160
2	1	1	3	2	1	3	2	0	2	3	2	1	3	640 788.517(0.100)	-0.06519
2	1	1	3	2	1	2	2	0	2	3	3	1	2	640 793.745(0.100)	-0.00903
2	1	1	3	3	1	2	2	0	2	3	2	1	2	640 799.061(0.100)	0.03280
2	1	1	3	3	1	3	2	0	2	3	3	1	3	640 804.861(0.100)	0.02749
2	1	1	3	3	1	4	2	0	2	3	3	1	4	640 809.536(0.100)	0.00173
2	1	1	3	2	1	2	2	0	2	3	3	1	3	640 816.075(0.100)	-0.19030
2	1	1	3	3	1	2	2	0	2	3	3	1	2	640 818.465(0.100)	0.11185
2	1	1	3	3	1	3	2	0	2	3	2	1	3	640 825.896(0.100)	-0.08381
2	1	1	3	2	1	2	2	0	2	3	2	1	3	640 837.348(0.100)	-0.06369
2	1	1	3	3	1	2	2	0	2	3	3	1	3	640 840.873(0.100)	0.00808
2	1	1	3	3	1	3	2	0	2	3	3	1	4	640 859.407(0.100)	-0.04760
2	1	1	2	2	1	2	2	0	2	2	2	1	3	645 111.178(0.100)	-0.07048
2	1	1	2	2	1	1	2	0	2	2	2	1	2	645 118.784(0.100)	-0.03407
2	1	1	2	2	1	2	2	0	2	2	2	1	2	645 142.843(0.100)	-0.06885
2	1	1	2	2	1	1	2	0	2	2	2	1	1	645 148.420(0.100)	-0.19977
2	1	1	2	2	1	3	2	0	2	2	2	1	3	645 150.805(0.100)	-0.06829
2	1	1	2	1	1	2	2	0	2	2	2	1	3	645 159.555(0.100)	-0.11288
2	1	1	2	2	1	2	2	0	2	2	2	1	1	645 173.299(0.100)	0.38419
2	1	1	2	2	1	2	2	0	2	2	1	1	2	645 173.299(0.100)	0.38419
2	1	1	2	1	1	1	2	0	2	2	2	1	1	645 180.728(0.100)	0.06478
2	1	1	2	1	1	1	2	0	2	2	1	1	2	645 180.728(0.100)	0.06478
2	1	1	2	1	1	2	2	0	2	2	2	1	2	645 191.191(0.100)	-0.14075
2	1	1	2	1	1	0	2	0	2	2	1	1	1	645 196.231(0.100)	-0.04154
2	1	1	2	2	1	1	2	0	2	2	1	1	0	645 206.745(0.100)	-0.05118
2	1	1	2	2	1	2	2	0	2	2	1	1	1	645 211.750(0.100)	0.00473
2	1	1	2	2	1	3	2	0	2	2	1	1	2	645 213.055(0.100)	0.00028
2	1	1	2	1	1	1	2	0	2	2	1	1	1	645 219.340(0.100)	-0.02789
2	1	1	2	1	1	2	2	0	2	2	2	1	1	645 221.750(0.100)	0.51794
2	1	1	2	1	1	2	2	0	2	2	1	1	2	645 221.750(0.100)	0.51794
2	1	1	2	1	1	1	2	0	2	2	1	1	0	645 238.429(0.100)	-0.08367
2	1	1	2	1	1	2	2	0	2	2	1	1	1	645 260.088(0.100)	-0.07677
2	1	1	2	2	1	1	2	0	2	3	3	1	2	646 818.042(0.100)	0.14697
2	1	1	2	2	1	2	2	0	2	3	3	1	3	646 864.569(0.100)	0.06762
2	1	1	2	2	1	2	2	0	2	3	2	1	3	646 885.610(0.100)	-0.03728
2	1	1	2	1	1	2	2	0	2	3	2	1	3	646 933.946(0.100)	-0.12137
2	1	1	2	2	1	3	2	0	2	3	3	1	4	646 958.718(0.100)	-0.02867

Notes. The complete version of the fit including all the measurements is available at the CDS: S1. ^(a) Following SPFIT format half-integer spins are rounded up to the next integer.

References

- Adande, G., & Ziurys, L. 2012, *ApJ*, **744**, 194
- Bailleux, S., Martin-Drumel, M., Margulès, L., et al. 2012, *A&A*, **538**, A135
- Bizzocchi, L., Caselli, P., & Dore, L. 2010, *A&A*, **510**, L5
- Bizzocchi, L., Caselli, P., Leonardo, E., & Dore, L. 2013, *A&A*, **555**, A109
- Brown, J., Chalkley, S., & Wayne, F. 1979, *Mol. Phys.*, **38**, 1521
- Brubach, J.-B., Manceron, L., Rouzières, M., et al. 2010, in WIRMS 2009 5th international workshop on infrared microscopy and spectroscopy with accelerator based sources, AIP Conf. Proc., 1214, 81
- Daniel, F., Gérin, M., Roueff, E., et al. 2013, *A&A*, **560**, A3
- Dislaire, V., Hily-Blant, P., Faure, A., et al. 2012, *A&A*, **537**, A20
- Fontani, F., Caselli, P., Palau, A., Bizzocchi, L., & Ceccarelli, C. 2015, *ApJ*, **808**, L46
- Füri, E., & Marty, B. 2015, *Nature Geoscience*, **8**, 515
- Gendriesch, R., Lewen, F., Winnewisser, G., & Müller, H. S. 2001, *J. Mol. Struct.*, **599**, 293
- Gerin, M., Marcelino, N., Biver, N., et al. 2009, *A&A*, **498**, L9
- Hily-Blant, P., Bonal, L., Faure, A., & Quirico, E. 2013a, *Icarus*, **223**, 582
- Hily-Blant, P., Des Forêts, G. P., Faure, A., Le Gal, R., & Padovani, M. 2013b, *A&A*, **557**, A65
- Kobayashi, K., Ozeki, H., Saito, S., Tonooka, M., & Yamamoto, S. 1997, *J. Chem. Phys.*, **107**, 9289
- Lis, D., Wootten, A., Gerin, M., & Roueff, E. 2010, *ApJ*, **710**, L49
- Margulès, L., Herbst, E., Ahrens, V., et al. 2002, *J. Mol. Spectr.*, **211**, 211
- Martin-Drumel, M., Pirali, O., Balcon, D., et al. 2011, *Rev. Sci. Instr.*, **82**, 113106
- Martin-Drumel, M., Pirali, O., & Vervloet, M. 2014, *J. Phys. Chem. A*, **118**, 1331
- Matsushima, F., Odashima, H., Iwasaki, T., Tsunekawa, S., & Takagi, K. 1995, *J. Mol. Struct.*, **352**, 371
- Morino, I., & Kawaguchi, K. 1997, *J. Mol. Spectr.*, **182**, 428
- Motiyenko, R., Margulès, L., Alekseev, E., Guillemin, J.-C., & Demaison, J. 2010, *J. Mol. Spectr.*, **264**, 94
- Müller, H. S., Klein, H., Belov, S. P., et al. 1999, *J. Mol. Spectr.*, **195**, 177
- Mumma, M. J., & Charnley, S. B. 2011, *ARA&A*, **49**, 471
- Ozeki, H., Bailleux, S., & Wlodarczak, G. 2011, *A&A*, **527**, A64
- Persson, C. M., De Luca, M., Mookerjee, B., et al. 2012, *A&A*, **543**, A145
- Persson, C. M., Olofsson, A. O. H., Le Gal, R., et al. 2016, *A&A*, **586**, A128
- Pickett, H. M. 1991, *J. Mol. Spectr.*, **148**, 371
- Roueff, E., Loison, J. C., & Hickson, K. M. 2015, *A&A*, **576**, A99
- Rousselot, P., Pirali, O., Jehin, E., et al. 2014, *ApJ*, **780**, L17
- Shinnaka, Y., Kawakita, H., Kobayashi, H., Nagashima, M., & Boice, D. C. 2014, *ApJ*, **782**, L16
- Steimle, T., Brown, J., & Curl Jr, R. 1980, *J. Chem. Phys.*, **73**, 2552